Table 1.4. Physical constants and frequently used quantities

Physical Constant/Quantity	Symbol	Quantity
charge of the electron	e	1.60219×10^{-19} C
mass of the electron	m_e	9.10953×10^{-31} kg
mass of the proton	m_p	1.67265×10^{-27} kg
mass of the neutron	m_n	1.67495×10^{-27} kg
unified atomic mass	u	1.66055×10^{-27} kg
speed of light in vacuum	c	2.99793×10^{8} m s^{-1}
Avogadro's constant	N_A	6.02205×10^{23} mol^{-1}

Table 1.5. Number Prefixes

a	f	p	n	μ	m	c	d	k	M	G
atto	femto	pico	nano	micro	milli	centi	deci	kilo	mega	giga
10^{-18}	10^{-15}	10^{-12}	10^{-9}	10^{-6}	10^{-3}	10^{-2}	10^{-1}	10^{3}	10^{6}	10^{9}

Reference List

Direct Reference

1. Enjalbal, C.; Maux, D.; Martinez, J.; Combarieu, R.; Aubagnac, J.-L. Mass Spectrometry and Combinatorial Chemistry: New Approaches for Direct Support-Bound Compound Identification. *Comb. Chem. High Throughput Screening* **2001,** *4*, 363-373.
2. Enjalbal, C.; Maux, D.; Combarieu, R.; Martinez, J.; Aubagnac, J.-L. Imaging Combinatorial Libraries by Mass Spectrometry: From Peptide to Organic-Supported Syntheses. *J. Comb. Chem.* **2003,** *5*, 102-109.
3. Maux, D.; Enjalbal, C.; Martinez, J.; Aubagnac, J.-L.; Combarieu, R. Static Secondary Ion Mass Spectrometry to Monitor Solid-Phase Peptide Synthesis. *J. Am. Soc. Mass Spectrom.* **2001,** *12*, 1099-1105.
4. Beverly, M.B.; Voorhees, K.J.; Hadfield, T.L. Direct Mass Spectrometric Analysis of Bacillus Spores. *Rapid Commun. Mass Spectrom.* **1999,** *13*, 2320-2326.
5. Jones, J.J.; Stump, M.J.; Fleming, R.C.; Lay, J.O., Jr.; Wilkins, C.L. Investigation of MALDI-TOF and FT-MS Techniques for Analysis of Escherichia Coli Whole Cells. *Anal. Chem.* **2003,** *75*, 1340-1347.
6. Fenselau, C.; Caprioli, R. Mass Spectrometry in the Exploration of Mars. *J. Mass Spectrom.* **2003,** *38*, 1-10.
7. He, F.; Hendrickson, C.L.; Marshall, A.G. Baseline Mass Resolution of Peptide Isobars: A Record for Molecular Mass Resolution. *Anal. Chem.* **2001,** *73*, 647-650.
8. Cooper, H.J.; Marshall, A.G. ESI-FT-ICR Mass Spectrometric Analysis of Wine. *J. Agric. Food. Chem.* **2001,** *49*, 5710-5718.
9. Hughey, C.A.; Rodgers, R.P.; Marshall, A.G. Resolution of 11,000 Compositionally Distinct Components in a Single ESI-FT-ICR Mass Spectrum of Crude Oil. *Anal. Chem.* **2002,** *74*, 4145-4149.
10. Mühlberger, F.; Wieser, J.; Ulrich, A.; Zimmermann, R. Single Photon Ionization Via Incoherent VUV-Excimer Light: Robust and Compact TOF Mass Spectrometer for Real-Time Process Gas Analysis. *Anal. Chem.* **2002,** *74*, 3790-3801.
11. Glish, G.L.; Vachet, R.W. The Basics of Mass Spectrometry in the Twenty-First Century. *Nat. Rev. Drug Discovery* **2003,** *2*, 140-150.
12. Busch, K.L. Synergistic Developments in MS. A 50-Year Journey From "Art" to Science. *Spectroscopy* **2000,** *15*, 30-39.
13. *Measuring Mass - From Positive Rays to Proteins;* Grayson, M.A., editor; ASMS and CHF: Santa Fe and Philadelphia, 2002.
14. Meyerson, S. Reminiscences of the Early Days of MS in the Petroleum Industry. *Org. Mass Spectrom.* **1986,** *21*, 197-208.

2.2.1 Electron Ionization

The classical procedure of ionization involves shooting energetic electrons on a neutral. This is called *electron ionization* (EI). Electron ionization has formerly been termed *electron impact ionization* or simply *electron impact* (EI). For EI, the neutral must previously have been transferred into the highly diluted gas phase, which is done by means of any sample inlet system suitable for the evaporation of the respective compound. In practice, the gas phase may be regarded highly diluted when the mean free path for the particles becomes long enough to make bimolecular interactions almost impossible within the lifetime of the particles concerned. This is easily achieved at pressures in the range of 10^{-4} Pa usually realized in electron ionization ion sources.

Here, the description of EI is restricted to what is essential for understanding the ionization process itself [18,19] and the consequences for the fate of the ions created. The practical aspects of EI and the interpretation of EI mass spectra are discussed later (Chaps. 5, 6).

2.2.1.1 Ions Generated by Electron Ionization

When a neutral is hit by an energetic electron carrying several tens of electronvolts (eV) of kinetic energy, some of the energy of the electron is transferred to the neutral. If the electron, in terms of energy transfer, collides very effectively with the neutral, the amount of energy transferred can effect ionization by ejection of one electron out of the neutral, thus making it a positive *radical ion*:

$$M + e^- \rightarrow M^{+\bullet} + 2e^- \tag{2.1}$$

EI predominantly creates singly charged ions from the precursor neutral. If the neutral was a molecule as in most cases, it started as having an even number of electrons, i.e., it was an *even-electron* (*closed-shell*) *molecule*. The molecular ion formed must then be a radical cation or an *odd-electron* (*open-shell*) *ion* as these species are termed, e.g., for methane we obtain:

$$CH_4 + e^- \rightarrow CH_4^{+\bullet} + 2e^- \tag{2.2}$$

In the rare case the neutral was a radical, the ion created by electron ionization would be even-electron, e.g., for nitric oxide:

$$NO^{\bullet} + e^- \rightarrow NO^+ + 2e^- \tag{2.3}$$

Depending on the analyte and on the energy of the primary electrons, doubly and even triply charged ions can also be observed. [20] In general, these are of low abundance.

$$M + e^- \rightarrow M^{2+} + 3e^- \tag{2.4}$$

$$M + e^- \rightarrow M^{3+\bullet} + 4e^- \tag{2.5}$$

While the doubly charged ion, M^{2+}, is an *even-electron ion*, the triply charged ion, $M^{3+\bullet}$, again is an *odd-electron ion*. In addition, there are several other events possible from the electron–neutral interaction, e.g., a less effective interaction will bring the neutral into an electronically excited state without ionizing it.

2.2.1.2 Ions Generated by Penning Ionization

Non-ionizing electron–neutral interactions create electronically excited neutrals. The ionization reactions occurring when electronically excited neutrals, e.g., noble gas atoms A*, collide with ground state species, e.g., some molecule M, can be divided into two classes. [21] The first process is *Penning ionization* (Eq. 2.6), [22] the second is *associative ionization* which is also known as the Hornbeck-Molnar process (Eq. 2.7). [23]

$$A^* + M \rightarrow A + M^{+\bullet} + e^- \quad (2.6)$$

$$A^* + M \rightarrow AM^{+\bullet} + e^- \quad (2.7)$$

Penning ionization occurs with the (trace) gas M having an ionization energy lower than the energy of the metastable state of the excited (noble gas) atoms A*. The above ionization processes have also been employed to construct mass spectrometer ion sources. [21,24] However, Penning ionization sources never escaped the realm of academic research to find widespread analytical application.

2.2.2 Ionization Energy

2.2.2.1 Definition of Ionization Energy

It is obvious that ionization of the neutral can only occur when the energy deposited by the electron–neutral collision is equal to or greater than the *ionization energy* (IE) of the corresponding neutral. Formerly, the ionization energy has been termed *ionization potential* (IP).

Definition: The *ionization energy* (IE) is defined as the minimum amount of energy which has to be absorbed by an atom or molecule in its electronic and vibrational ground states form an ion that is also in its ground states by ejection of an electron.

2.2.2.2 Ionization Energy and Charge-Localization

Removal of an electron from a molecule can formally be considered to occur at a σ-bond, a π-bond or at a lone electron pair with the σ-bond being the least favorable and the lone electron pair being the most favorable position for *charge-localization* within the molecule. This is directly reflected in the IEs of molecules (Table 2.1). Nobel gases do exist as atoms having closed electron shells and there-

Table 2.1. Ionization energies of selected compounds[a]

Compound	IE[b] [eV]	Compound	IE[b] [eV]
hydrogen, H_2	15.4	helium, He	24.6
methane, CH_4	12.6	neon, Ne	21.6
ethane, C_2H_6	11.5	argon, Ar	15.8
propane, n-C_3H_8	10.9	krypton, Kr	14.0
butane, n-C_4H_{10}	10.5	xenon, Xe	12.1
pentane, n-C_5H_{12}	10.3		
hexane, n-C_6H_{14}	10.1	nitrogen, N_2	15.6
decane, n-$C_{10}H_{22}$	9.7	oxygen, O_2	12.1
		carbonmonoxide, CO	14.0
ethene, C_2H_4	10.5	carbondioxide, CO_2	13.8
propene, C_3H_6	9.7		
(E)-2-butene, C_4H_8	9.1	fluorine, F_2	15.7
		chlorine, Cl_2	11.5
benzene, C_6H_6	9.2	bromine, Br_2	10.5
toluene, C_6H_8	8.8	iodine, I_2	9.3
indene, C_9H_8	8.6		
naphthalene, $C_{10}H_8$	8.1	ethanol, C_2H_6O	10.5
biphenyl, $C_{12}H_{10}$	8.2	dimethylether, C_2H_6O	10.0
anthracene, $C_{14}H_{10}$	7.4	ethanethiol, C_2H_6S	9.3
aniline, C_6H_7N	7.7	dimethyldisulfide, $C_2H_6S_2$	8.7
triphenylamine, $C_{18}H_{15}N$	6.8	dimethylamine, C_2H_7N	8.2

[a] IE data extracted from Ref. [28] with permission. © NIST 2002.
[b] All values have been rounded to one digit.

2.3 Vertical Transitions

Electron ionization occurs extremely fast. The time needed for an electron of 70 eV to travel 1 nm distance, i.e., roughly half a dozen bonds, through a molecule is only about 2×10^{-16} s and even larger molecules can be traversed on the low femtosecond scale. The molecule being hit by the electron can be seen at rest because the thermal velocity of a few 100 m s^{-1} is negligible compared to the speed of the electron rushing through. Vibrational motions are slower by at least two orders of magnitude, e.g., even the fast C–H stretching vibration takes 1.1×10^{-14} s per cycle as can be calculated from its absorbance around 3000 cm^{-1} in infrared spectra. According to the *Born-Oppenheimer approximation*, the electronic motion and the nuclear motion can therefore be separated, i.e., the positions of the atoms and thus bond lengths do not change while ionization takes place. [29,30] In addition, the *Franck-Condon principle* states that the probability for an electronic transition is highest where the electronic wave functions of both ground state and ionized state have their maxima. [31,32] This gives rise to *vertical transitions*.

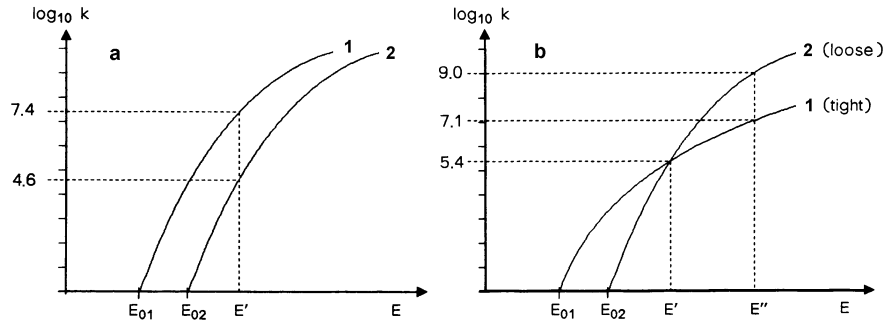

Fig. 2.7. Comparison of different types of reactions by their $k_{(E)}$ functions. Reactions of the same type show $k_{(E)}$ functions that are "parallel" (**a**), whereas $k_{(E)}$ functions of different types tend to cross over at intermediate excess energy (**b**). In **a** reaction **1** would proceed $10^{2.8}$ (630) times faster at an internal energy E' than would reaction **2**. In **b** both reactions have the same rate constant, $k = 10^{5.4}$ s^{-1}, at an internal energy E', whereas reaction **2** becomes $10^{1.9}$ (80) times faster at E''.

2.6.5 Practical Consequences of Internal Energy

Even comparatively small molecular ions can exhibit a substantial collection of first, second, and higher generation fragmentation pathways due their internal energy. [40] The fragmentation pathways of the same generation are competing with each other, their products being potential precursors for the next generation of fragmentation processes (Figs. 2.4 and 2.8).

The hypothetical molecular ion ABYZ$^{+\bullet}$, for example, might show three possible first generation fragmentation pathways, two of them proceeding by rearrangement, one by simple cleavage of a bond. There are three first generation fragment ions which again have several choices each. The second generation fragment ions Y$^{+\bullet}$ and YZ^{+} are even formed on two different pathways each, a widespread phenomenon. In an EI mass spectrum of ABYZ, all ionic species shown would be detected (Chap. 5.1.4).

Fragmentation trees similar to that shown here can be constructed from any EI mass spectrum, providing ten thousands of examples for the sixth assumption of QET that fragment ions may again be subject to dissociation, provided their internal energy suffices.

Note: The assumptions of QET have turned into basic statements governing the behavior of isolated ions in the gas phase and thus, in mass spectrometry in general.

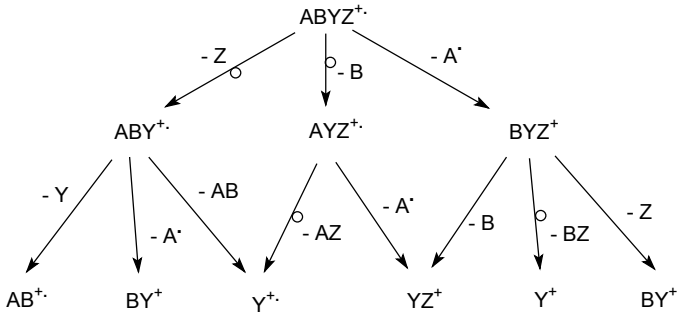

Fig. 2.8. Possible fragmentation pathways for hypothetical molecular ions ABYZ$^{+\bullet}$ having internal energies typical for EI.

2.7 Time Scale of Events

A mass analyzer normally brings only those ions to detection that have been properly formed and accelerated by the ion source beforehand (Chap. 4). Therefore, a reaction needs to proceed within a certain period of time – the dwelltime of ions within the ion source – to make the products detectable in the mass spectrum, and for this purpose there is a need for some excess energy in the transition state.

The dwelltime of ions within the ion source is defined by the extraction voltages applied to accelerate and focus them into an ion beam and by the dimensions of that ion source. In standard EI ion sources the freshly formed ions dwell about 1 µs before they are forced to leave the ionization volume by action of the accelerating potential. [41] As the ions then travel at speeds of some 10^4 m s^{-1} they pass the mass analyzer in the order of 10–50 µs (Fig. 2.9). [9] Even though this illustration has been adapted for a double focusing magnetic sector mass spectrometer, an ion of *m/z* 100, and an acceleration voltage of 8 kV, the effective time scales for other types of instruments (quadrupole, time-of-flight) are very similar under their typical conditions of operation (Table 2.4).

Table 2.4. Typical ion flight times in different types of mass spectrometers

Mass Analyzer	Flight Path [m]	Acceleration Voltage [V]	Typical *m/z*	Flight Time [µs]
quadrupole	0.2	10	500	57
magnetic sector	2.0	5000	500	45
time-of-flight	2.0	20,000	2000	45

predominating fragment ion, corresponds to a region of the internal energy distribution which has a low ion population. This explains why $[C_3H_7]^+$ constitutes the base peak of the spectrum. Beyond 5 eV internal energy, the $[C_3H_5]^+$ ion, *m/z* 41, becomes the most prominent fragment ion.

2.11 Gas Phase Basicity and Proton Affinity

Not all ionization methods rely on such strictly unimolecular conditions as EI does. Chemical ionization (CI, Chap. 7), for example, makes use of reactive collisions between ions generated from a reactant gas and the neutral analyte to achieve its ionization by some bimolecular process such as proton transfer. The question which reactant ion can protonate a given analyte can be answered from *gas phase basicity* (GB) or *proton affinity* (PA) data. Furthermore, proton transfer, and thus the relative proton affinities of the reactants, play an important role in many ion-neutral complex-mediated reactions (Chap. 6.12).

2.11.1 Definition of Gas Phase Basicity and Proton Affinity

Proton affinity and gas *phase basicity* are thermodynamic quantities. Consider the following gas phase reaction of a (basic) molecule, B:

$$B_g + H_g^+ \rightarrow [BH]_g^+ \tag{2.34}$$

The tendency of B to accept a proton is then quantitatively described by

$$-\Delta G_r^0 = GB_{(B)} \quad \text{and} \quad -\Delta H_r^0 = PA_{(B)}, \tag{2.35}$$

i.e. the gas phase basicity $GB_{(B)}$ is defined as the negative free energy change for the proton transfer, $-\Delta G_r^0$, whereas the proton affinity $PA_{(B)}$ is the negative enthalpy change, $-\Delta H_r^0$, for the same reaction. [100,101] From the relation

$$\Delta G^0 = \Delta H^0 - T\,\Delta S^0 \tag{2.36}$$

we obtain the expression

$$PA_{(B)} = GB_{(B)} - T\,\Delta S^0 \tag{2.37}$$

with the entropy term $T\Delta S^0$ usually being relatively small (25–40 kJ mol^{-1}). Furthermore, in case of an equilibrium

$$[AH]^+ + B \rightleftharpoons A + [BH]^+ \tag{2.38}$$

with the equilibrium constant K_{eq} for which we have

$$K_{eq} = [BH^+]/[AH^+] \cdot [A]/[B] \tag{2.39}$$

the gas phase basicity is related to K_{eq} by [102,103]

$$GB_{(B)} = -\Delta G^0 = RT \ln K_{eq} \tag{2.40}$$

2.11.2 Determination of Gas Phase Basicities and Proton Affinities

The methods for the determination of GBs and PAs make use of their relation to K_{eq} (Eq. 2.40) and the shift of K_{eq} upon change of $[AH]^+$ or B, respectively. [101,103] Basically, the value of GB or PA is bracketed by measuring K_{eq} with a series of several reference bases ranging from lower to higher GB than the unknown. There are two methods we should address in brief, a detailed treatment of the topic being beyond the scope of the present book, however.

2.11.2.1 Kinetic Method

The *kinetic method* [102,104-106] compares the relative rates of the competitive dissociations of a proton-bound adduct $[A–H–B]^+$ formed by admitting a mixture of A and B to a CI ion source. [104,105] There, the proton-bound adduct $[A–H–B]^+$ is generated amongst other products such as $[AH]^+$ and $[BH]^+$. Using standard tandem MS techniques, e.g., MIKES, the cluster ion $[A–H–B_{ref}]^+$ is selected and allowed to undergo metastable decomposition:

$$[AH]^+ + B_{ref} \leftarrow [A–H–B_{ref}]^+ \rightarrow A + [B_{ref}H]^+ \qquad (2.41)$$

The relative intensities of the products $[AH]^+$ and $[B_{ref}H]^+$ are then used as a measure of relative rate constants of the competing reactions. In case the PA of the unknown was equal to that of the reference, both peaks would be of equal intensity. As this will almost never be the case, a series of reference bases is employed instead, and PA is determined by interpolation. The value of $PA_{(A)}$ is obtained from a plot of $\ln[AH]^+/[B_{ref}H]^+$ versus $PA_{(B)}$ at $\ln[AH]^+/[B_{ref}H]^+ = 0$.

2.11.2.2 Thermokinetic Method

The *thermokinetic method* [107,108] uses the measurement of the forward rate constant of the equilibrium

$$[AH]^+ + B_{ref} \rightleftharpoons A + [B_{ref}H]^+ \qquad (2.42)$$

The thermokinetic method takes advantage of the correlation observed between k_{exp} and $\Delta G_2^{\,0}$ through the relationship

$$\frac{k_{exp}}{k_{coll}} = \frac{1}{1 + exp(\Delta G_2^0 + \Delta G_a^0)/RT} \qquad (2.43)$$

where k_{coll} is the collision rate constant and $\Delta G_a^{\,0}$ a term close to RT. The GB of the unknown is then obtained from $\Delta G_2^{\,0} = GB - GB_{ref}$. The task to establish a proper value of the reaction efficiency $RE = k_{exp}/k_{coll}$, is solved by plotting the experimental values of RE versus $GB_{(B)}$ and interpolating these points with a parametric function. Although this can be done with high accuracy, it is still a matter of debate which value of RE yields the most realistic GB, suggestions being $RE = 0.1–0.5$. [101]

an *U*/*V* = *constant* linked scan is obtained allowing ions of increasingly higher *m/z* values to travel through the quadrupole.

Overall, the quadrupole analyzer rather acts as a mass filter than as a momentum (B sector) or energy (ESA) spectrometer; hence the widespread use of the term *quadrupole mass filter*.

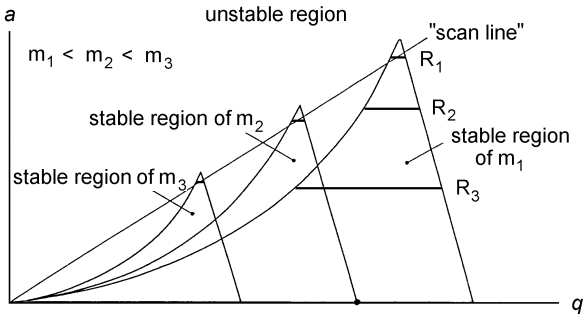

Fig. 4.35. Scanning of linear quadrupoles means performing a *U*/*V* = *constant* linked scan. Resolution is adjusted by variation of the *a*/*q* ratio: higher *a*/*q* ratio means higher resolution, and is represented by a steeper "scan line"; $R_1 > R_2 > R_3$.

Note: Scanning of any quadrupole means shifting the whole stability diagram along a "scan line", because each *m/z* value has a stability diagram of its own (Figs. 4.34, 4.35). The representation of a scan by a "scan line" would only be correct in case of infinite resolution, i.e., if the apices were connected. Any real resolution is represented by a horizontal line across the stability region, where only ions falling in the region above that line are transmitted.

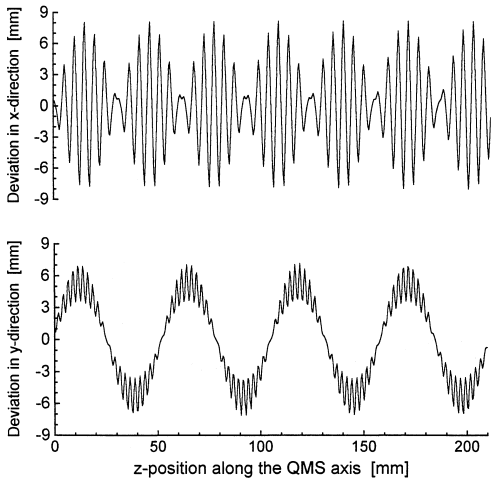

Fig. 4.36. Projection of a 3D trajectory simulation of a stable ion onto the *x*- and *y*-coordinate. Reproduced from Ref. [110] with permission. © Elsevier Science, 1998.

detector as still intact molecular ions. The fragmentation pathways of the same generation are competing with each other, their products being potential precursors for the next generation of fragmentation processes.

Example: Imagine the hypothetical molecular ion $ABYZ^{+\bullet}$ undergoing three competing first generation fragmentations, two of them rearrangements, one a homolytic bond cleavage (Fig. 5.5). Next, three first generation fragment ions have several choices each, and thus the second generation fragment ions $Y^{+\bullet}$ and YZ^{+} are both formed on two different pathways. The formation of the same higher generation fragment ion on two or more different pathways is a widespread phenomenon. A closer look reveals that $Y^{+\bullet}$ and Y^{+} are different although having identical empirical formulas, because one of them is an odd-electron and the other an even-electron species. Nevertheless, they would both contribute to one common peak at the same nominal *m/z* in a mass spectrum of ABYZ (Chap. 3.1.4).

In an EI mass spectrum of ABYZ, all ionic species formed as a result of numerous competing and consecutive reactions would be detected, but there is no simple rule which of them should give rise to intensive peaks and which of them would be almost overlooked.

Obviously, the first generation fragment ions should be more closely related to the initial structure of ABYZ than those of the second or even third generation. Fortunately, such higher generation (and therefore low-mass) fragment ions can also reveal relevant information on the constitution of the analyte. In particular, they yield reliable information on the presence of functional groups (Chap. 6).

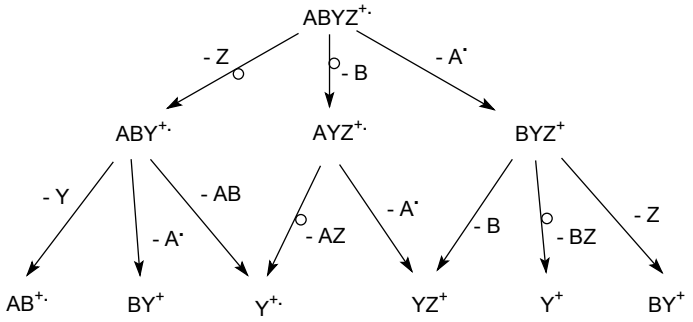

Fig. 5.5. Possible fragmentation pathways for hypothetical molecular ions $ABYZ^{+\bullet}$ having internal energies in the range typical for EI.

5.1.5 Low-Energy Electron Ionization Mass Spectra

The excess energy deposited onto a molecular ion can obviously be decreased at low electron energy. The use of 12–15 eV electrons instead of the routinely employed 70 eV electrons still allows to ionize most analytes while reducing disadvantageous fragmentation, e.g., the EI mass spectra of large hydrocarbons benefit from such measures. [12] Especially in conjunction with low ion source tempera-

tral intermediates and products in the dissociation reactions of many ionized molecules. Further, it seems now likely that the long-lived molecular ions of many organic compounds may exist as their distonic forms. [43] It has been shown, for example, that the long-lived radical ions of simple organophosphates spontaneously isomerize to distonic isomers, [47] and that the ring-opening product of cyclopropane molecular ion is also distonic. [48] The next distonic ions we are going to learn about are the intermediates of the McLafferty rearrangement (Chap. 6.7).

6.4 Benzylic Bond Cleavage

The α-cleavage in molecular ions of ketones, amines, ethers and similar functionalized compounds yields specific cleavage products of high importance for structure elucidation. Analogous behavior is observed in the mass spectra of phenylalkanes. [49]

6.4.1 Cleavage of the Benzylic Bond in Phenylalkanes

Molecular ions of phenylalkanes are comparatively stable due to the good charge stabilizing properties of the aromatic ring and thus, they normally give rise to intense peaks. Those molecular ions, possessing a benzylic bond preferably show

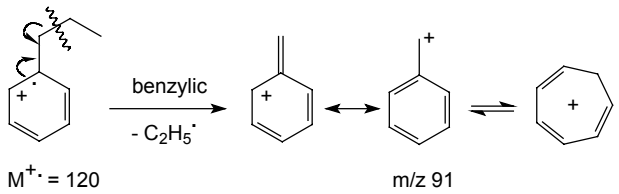

Scheme 6.22.

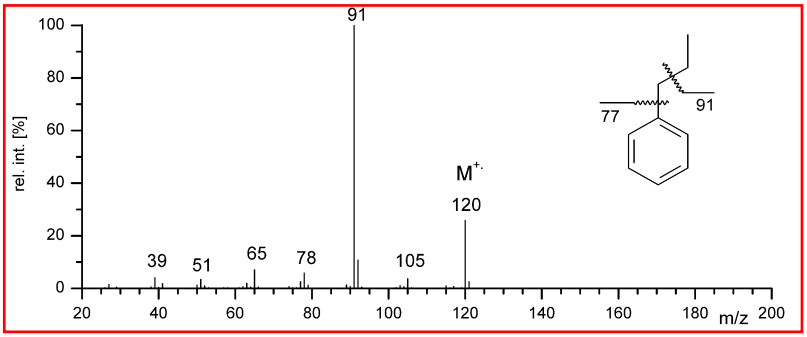

Fig. 6.14. EI mass spectrum of *n*-propylbenzene. The molecular ion peak and the primary fragment ion have significant intensity, whereas low-mass fragments are less abundant. Spectrum used by permission of NIST. © NIST 2002.

tomers, in which the keto forms are generally more stable. [92] The experimental findings also are in good agreement with MNDO calculations, [93] and support the hypothesis that reketonization does not play a major role for further fragmentation. Anyway, it is helpful to remind the possible tautomerization when seeking for subsequent decomposition pathways.

6.7.1.2 The Role of the γ-Hydrogen for the McLafferty Rearrangement

The occurrence of the McLafferty rearrangement is strictly limited to molecular ions possessing at least one γ-hydrogen for transfer to the terminal atom at the double bond. Thus, blocking the γ-position, e.g., by introduction of alkyl or halogen substituents, effectively hinders this dissociation pathway.

Example: In the EI mass spectrum of 3,3-dimethyl-2-butanone no fragment ion due to McLafferty rearrangement can be observed, because there is no γ-hydrogen available (Fig. 6.23). Instead, the products are exclusively formed by simple cleavages as evident from their odd-numbered *m/z* values. The highly stable *tert*-butyl ion, *m/z* 57, predominates over the acylium ion at *m/z* 43 (Chap. 6.6.2).

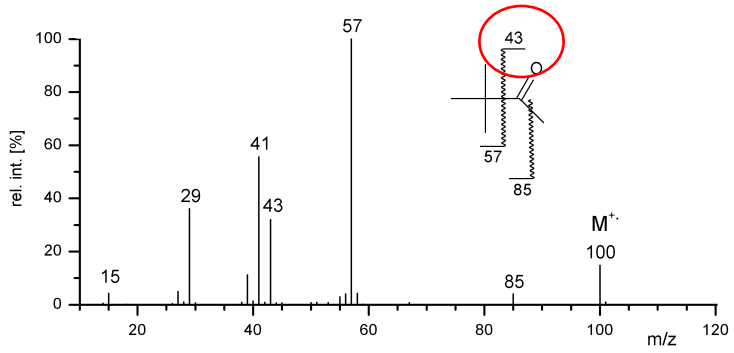

Fig. 6.23. EI spectrum of 3,3-dimethyl-2-butanone. The McLafferty rearrangement issuppressed, because there is no γ-hydrogen. Spectrum by permission of NIST. © NIST 2002.

6.7.2 Fragmentation of Carboxylic Acids and Their Derivatives

The mass spectra of carboxylic acids and their derivatives are governed by both α-cleavage and McLafferty rearrangement. As expected, α-cleavage may occur at either side of the carbonyl group causing $OH^{\bullet}$ loss, $[M–17]^+$, or alternatively alkyl loss. Whereas the α-cleavages can even be observed for formic acid where they are leading to $[M–OH]^{+\bullet}$, *m/z* 29, $[M–H]^{+\bullet}$, *m/z* 45, and the respective charge migration products (Fig. 6.24), the McLafferty rearrangement can only occur from butanoic acid and its derivatives onwards. [82,84] Analogous to aliphatic aldehydes, the same fragment ions are obtained for a homologous series of carboxylic acids, provided they are not branched at the α-carbon. Thus, highly characteristic fragment ions make their recognition straightforward.

Example: The molecular ion of dipentyl terephthalate either fragments by α-cleavage to yield the $[M–RO]^+$ fragment ion, *m/z* 219, or by double hydrogen transfer causing the *m/z* 237 peak (Fig. 6.30). It is worth noting that there is no signal due to McLafferty rearrangement as might be expected at first sight. Even more interestingly, both of the above fragments are capable of pentene loss which is detected at *m/z* 149 and 167, respectively. This indicates that they may undergo McLafferty rearrangement although being even-electron ions. [86] The spectrum of the deuterium-labeled isotopomer reveals that there is no hydrogen scrambling preceding the α-cleavage, because the peak is completely shifted by 2 u to higher mass, *m/z* 221. The rearrangement, on the other hand, causes two peaks, one corresponding to *r2H* , *m/z* 239, and one corresponding to *rHD*, *m/z* 240.

6.7.4.1 Double Hydrogen Transfer of Phthalates

The fragment ions at *m/z* 149, $[C_8H_5O_3]^+$, and 167, $[C_8H_7O_4]^+$, are especially prominent in the EI spectra of phthalates. The formation of the $[C_8H_5O_3]^+$ ion has initially been attributed to a McLafferty rearrangement followed by loss of an alkoxy radical and final stabilization to a cyclic oxonium ion. [104] However, it has been revealed that four other pathways in total lead to its formation excluding the above one. [105,106] The two most prominent fragmentation pathways are:

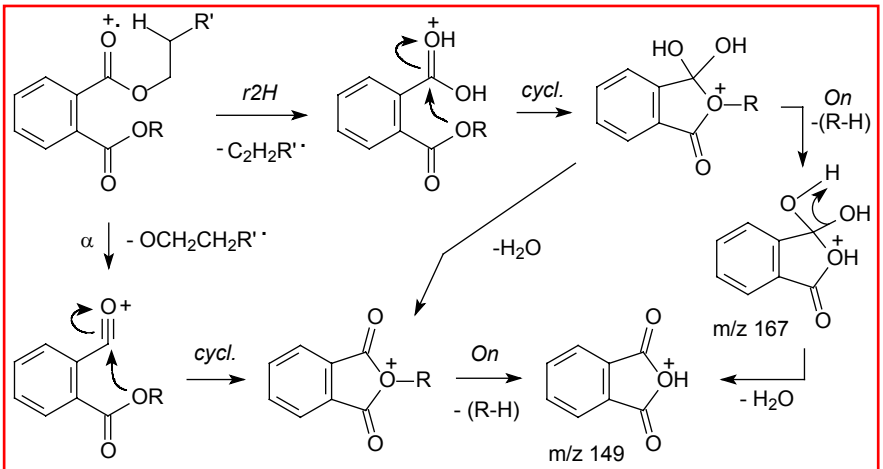

Scheme 6.45.

Note: Phthalates, especially di-2-ethylhexyl phthalate (also known as dioctyl phthalate, DOP), are commonly used plasticizers in synthetic polymers. Unfortunately, they are extracted from the polymer upon exposure to solvents such as dichloromethane, chloroform or toluene, e.g., from syringes, tubing, vials etc. Therefore, they are often detected as impurities. They are easily recognized from their peaks at *m/z* 149 (often base peak), *m/z* 167, and $[M–(R–2H)]^+$ (*m/z* 279 in case of DOP). The molecular ion is often absent in their EI spectra.

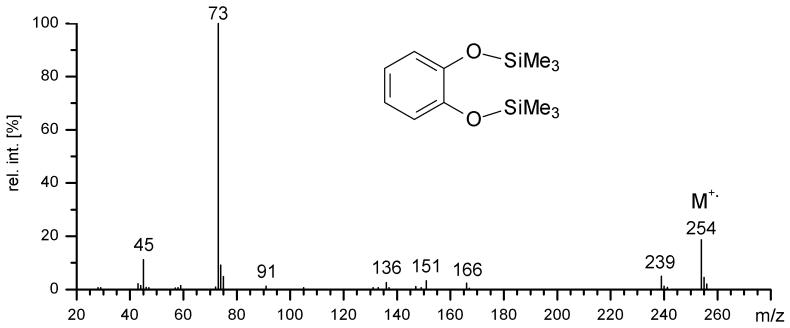

Fig. 6.48. EI mass spectrum of 1,2-bis(trimethylsiloxy)benzene. The isotopic pattern of silicon is clearly visible in the signals at *m/z* 73, 239, and 254 (Chap. 3.2.6). Spectrum used by permission of NIST. © NIST 2002.

Note: Trimethylsilylether (TMS) derivatives are frequently employed to volatize alcohols, [14,203] carboxylic acids, [204,205] and other compounds [206,207] for mass spectrometry, and for GC-MS applications in particular. The EI mass spectra of TMS derivatives exhibit weak molecular ion peaks, clearly visible $[M–CH_3]^+$ signals and often $[Si(Me)_3]^+$, *m/z* 73, as the base peak.

6.13.3 *Ortho* Elimination in the Fragmentation of Nitroarenes

6.13.3.1 Fragmentation of Nitroarenes

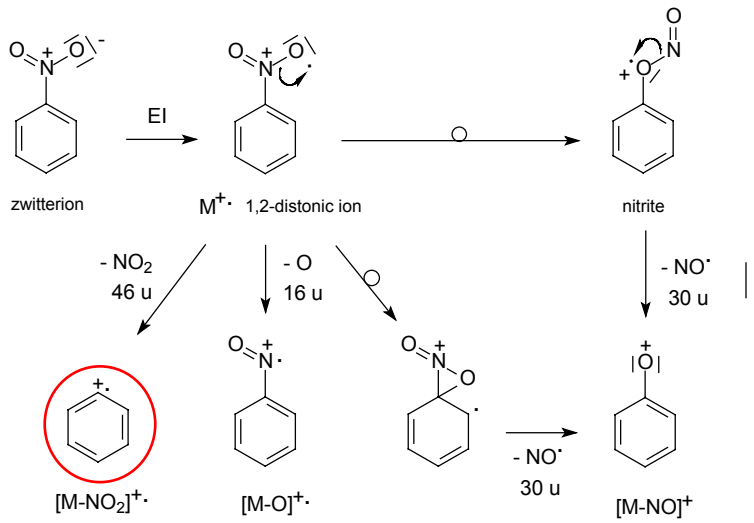

Scheme 6.72.

from ionizing primary electrons which is important to suppress competing direct EI of the analyte. There are four general pathways to form ions from a neutral analyte M in CI:

$M + [BH]^+ \rightarrow [M+H]^+ + B$	*proton transfer*	(7.1)
$M + X^+ \rightarrow [M+X]^+$	*electrophilic addition*	(7.2)
$M + X^+ \rightarrow [M-A]^+ + AX$	*anion abstraction*	(7.3)
$M + X^{+\bullet} \rightarrow M^{+\bullet} + X$	*charge exchange*	(7.4)

Although proton transfer is generally considered to yield protonated analyte molecules, $[M+H]^+$, acidic analytes may also form abundant $[M-H]^-$ ions by protonating some other neutral. Electrophilic addition chiefly occurs by attachment of complete reagent ions to the analyte molecule, e.g., $[M+NH_4]^+$ in case of ammonia reagent gas. Hydride abstractions are abundant representatives of anion abstraction, e.g., aliphatic alcohols rather yield $[M-H]^+$ ions than $[M+H]^+$ ions. [11,12] Whereas reactions 7.1–7.3 result in even electron ions, charge exchange (Eq. 7.4) yields radical ions of low internal energy which behave similar to molecular ions in low-energy electron ionization (Chap. 5.1.5).

Note: It is commonplace to denote $[M+H]^+$ and $[M-H]^+$ ions as *quasimolecular ions* because these ions comprise the otherwise intact analyte molecule and are detected instead of a molecular ion when CI or other soft ionization methods are employed. Usually, the term is also applied to $[M+alkali]^+$ ions created by other soft ionization methods.

7.1.2 Chemical Ionization Ion Sources

CI ion sources exhibit close similarity to EI ion sources (Chap. 5.2.1). In fact, modern EI ion sources can usually be switched to CI operation in seconds, i.e., they are constructed as *EI/CI combination ion sources*. Such a change requires the EI ion source to be modified according to the needs of holding a comparatively high pressure of reagent gas (some 10^2 Pa) without allowing too much leakage into the ion source housing. [13] This is accomplished by axially inserting some inner wall, e.g., a small cylinder, into the ion volume leaving only narrow holes for the entrance and exit of the ionizing primary electrons, the inlets and the exiting ion beam. The ports for the reference inlet, the gas chromatograph (GC) and the direct probe (DIP) need to be tightly connected to the respective inlet system during operation, i.e., an empty DIP is inserted even when another inlet actually provides the sample flow into the ion volume. The reagent gas is introduced directly into the ion volume to ensure maximum pressure inside at minimum losses to the ion source housing (Fig. 7.1). During CI operation, the pressure in the ion source housing typically rises by a factor of 20–50 as compared to the background pressure of the instrument, i.e., to 5×10^{-4}–10^{-3} Pa. Thus, sufficient pumping

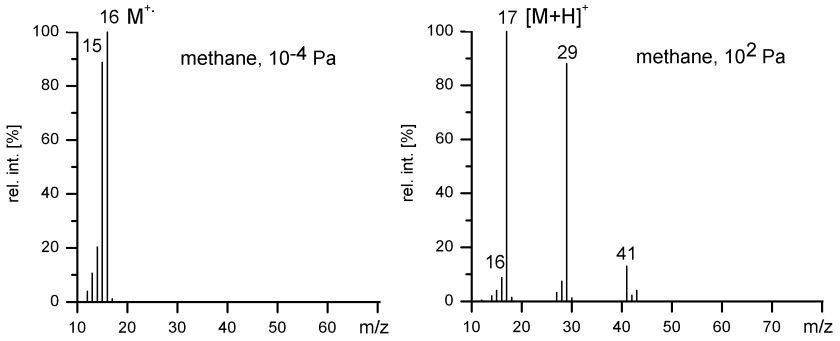

Fig. 7.2. Comparison of the methane spectrum upon electron ionization at different ion source pressures: (**a**) approx. 10^{-4} Pa, (**b**) approx. 10^{2} Pa. The latter represents the typical methane reagent gas spectrum in positive-ion CI.

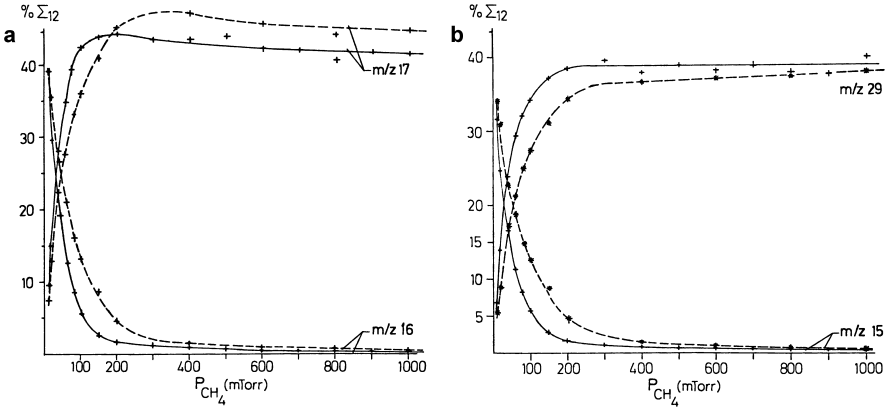

Fig. 7.3. Percentage of total ionization above *m/z* 12 (% Σ_{12}) of (**a**) $CH_4^{+\bullet}$, *m/z* 16, and CH_5^+, *m/z* 17, and (**b**) CH_3^+, *m/z* 15, and $C_2H_5^+$, *m/z* 29, as a function of CH_4 pressure at 100 eV electron energy and at ion source temperatures 50 °C (——) and 175 °C (-----); 100 mTorr = 13.33 Pa. Adapted from Ref. [19] by permission. © Elsevier Science, 1990.

7.2.2.1 CH_5^+ and Related Ions

The protonated methane ion, CH_5^+, represents a reactive as well as fascinating species in the methane reagent gas plasma. Its structure has been calculated and experimentally verified. [16] The chemical behavior of the CH_5^+ ion appears to be compatible with a stable structure, involving a three-center two-electron bond associating 2 hydrogens and the carbon atom. Rearrangement of this structure due to exchange between one of these hydrogens and one of the three remaining hydrogens appears to be a fast process that is induced by interactions with the chemical ionization gas. In case of the $C_2H_7^+$ intermediate during $C_2H_5^+$ ion formation sev-

eral isomerizing structures are discussed. [17,18] In protonated fluoromethane, the conditions are quite different, promoting a weak C–F and a strong F–H bond. [20]

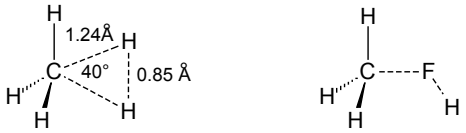

Scheme 7.1.

7.2.3 Energetics of Protonation

The tendency of a (basic) molecule B to accept a proton is quantitatively described by its *proton affinity* PA (Chap. 2.11). For such a protonation we have: [3]

$$B_g + H_g^+ \rightarrow [BH]_g^+; \qquad -\Delta H_r^0 = PA_{(B)} \tag{7.12}$$

In case of an intended protonation under the conditions of CI one has to compare the PAs of the neutral analyte M with that of the complementary base B of the proton-donating reactant ion $[BH]^+$ (Brønsted acid). Protonation will occur as long as the process is exothermic, i.e., if $PA_{(B)} < PA_{(M)}$. The heat of reaction has basically to be distributed among the degrees of freedom of the $[M+H]^+$ analyte ion. [12,21] This means in turn, that the minimum internal energy of the $[M+H]^+$ ions is determined by:

$$E_{int(M+H)} = -\Delta PA = PA_{(M)} - PA_{(B)} \tag{7.13}$$

Some additional thermal energy will also be contained in the $[M+H]^+$ ions. Having PA data at hand (Table 2.6) one can easily judge whether a reagent ion will be able to protonate the analyte of interest and how much energy will be put into the $[M+H]^+$ ion.

Example: The CH_5^+ reactant ion will protonate C_2H_6 because Eq. 7.13 gives $\Delta PA = PA_{(CH4)} - PA_{(C2H6)} = 552 - 601 = -49$ kJ mol^{-1}. The product, protonated ethane, $C_2H_7^+$, immediately stabilizes by H_2 loss to yield $C_2H_5^+$. [17,18] In case of tetrahydrofurane, protonation is more exothermic: $\Delta PA = PA_{(CH4)} - PA_{(C4H8O)} = 552 - 831 = -279$ kJ mol^{-1}.

7.2.3.1 Impurities of Higher PA than the Reagent Gas

Due to the above energetic considerations, impurities of the reagent gas having a higher PA than the neutral reagent gas are protonated by the reactant ion. [3] Residual water is a frequent source of contamination. Higher concentrations of water in the reagent gas may even alter its properties completely, i.e., H_3O^+ becomes the predominant species in a CH_4/H_2O mixture under CI conditions (Fig. 7.4). [22]

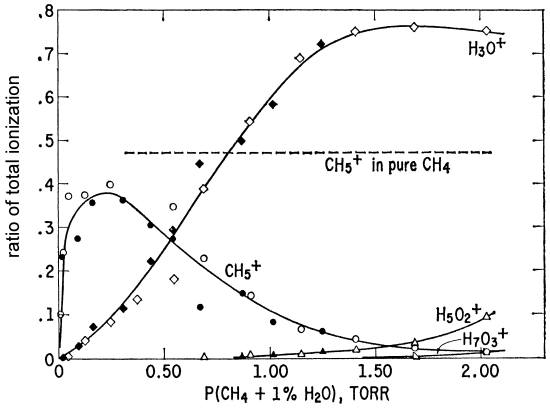

Fig. 7.4. Relative concentrations of CH_5^+ and H_3O^+ ions vs. pressure of a mixture of CH_4 (99 %) and H_2O (1 %). 1 Torr = 133 Pa. Reproduced from Ref. [22] by permission. © American Chemical Society, 1965.

Note: Any analyte of suitable PA may be regarded as basic impurity of the reagent gas, and therefore becomes protonated in excellent yield. Heteroatoms and π-electron systems are the preferred sites of protonation. Nevertheless, the additional proton often moves between several positions of the ion, sometimes accompanied by its exchange with otherwise fixed hydrogens. [23,24]

7.2.4 Methane Reagent Gas PICI Spectra

The $[M+H]^+$ quasimolecular ion in methane reagent gas PICI spectra – generally denoted *methane-CI spectra* – is usually intense and often represents the base peak. [25-27] Although protonation in CI is generally exothermic by 1–4 eV, the degree of fragmentation of $[M+H]^+$ ions is much lower than that observed for the same analytes under 70 eV EI conditions (Fig. 7.5). This is because $[M+H]^+$ ions have i) a narrow internal energy distribution, and ii) fast radical-induced bond cleavages are prohibited, because solely intact molecules are eliminated from these even-electron ions.

Occasionally, hydride abstraction may occur instead of protonation. Electrophilic addition fairly often gives rise to $[M+C_2H_5]^+$ and $[M+C_3H_5]^+$ adduct ions. Thus, [M+29] and [M+41] peaks are sometimes observed in addition to the expected – usually clearly dominating – [M+1] peak.

Note: Hydride abstraction is only recognized with some difficulty. To identify a $[M–H]^+$ peak occurring instead of a $[M+H]^+$ peak it is useful to examine the mass differences between the signal in question and the products of electrophilic addition. In such a case, [M+29] and [M+41] peaks are observed as seemingly [M+31] and [M+43] peaks, respectively. An apparent loss of 16 u might indicate an $[M+H–H_2O]^+$ ion instead of an $[M+H–CH_4]^+$ ion.

fragment ion peaks that can be assigned as $[M+H–H_2O]^+$, *m/z* 163; $[M+H–H_2C=CO]^+$, *m/z* 139; and $[M+H–CH_3COOH]^+$, *m/z* 121. In addition to the $[M+H]^+$ ion at *m/z* 180, phenacetin forms a $[2M+H]^+$ cluster ion, *m/z* 359. Such $[2M+H]^+$ cluster ions are frequently observed in CI-MS.

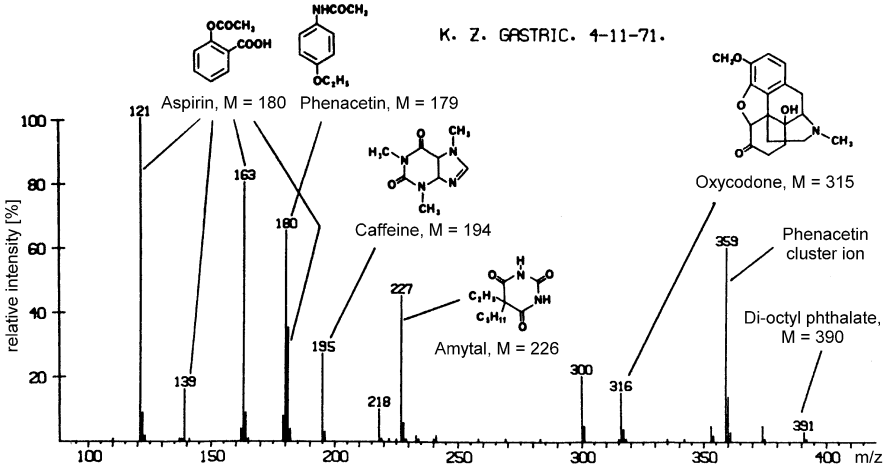

Fig. 7.8. Isobutane CI mass spectrum of gastric contents in an overdose case. Reproduced from Ref. [29] by permission. © American Chemical Society, 1970.

Table 7.1. Common PICI reagent gases

Reagent Gas	Reactant Ions	Neutral from Reactant Ions	PA of Neutral Product	Analyte Ions
H_2	H_3^+	H_2	424	$[M+H]^+$, $[M–H]^+$
CH_4	CH_5^+, ($C_2H_5^+$ and $C_3H_5^+$)	CH_4	552	$[M+H]^+$ ($[M+C_2H_5]^+$ and $[M+C_3H_5]^+$)
i-C_4H_{10}	*t*-$C_4H_9^+$	*i*-C_4H_8	820	$[M+H]^+$, ($[M+C_4H_9]^+$, eventually $[M+C_3H_3]^+$, $[M+C_3H_5]^+$ and $[M+C_3H_7]^+$)
NH_3	NH_4^+	NH_3	854	$[M+H]^+$, $[M+NH_4]^+$

Note: Resulting from the large excess of the reagent gas, its spectrum is of much higher intensity than that of the analyte. Therefore, CI spectra are usually acquired starting above the *m/z* range occupied by reagent ions, e.g., above *m/z* 50 for methane or above *m/z* 70 for isobutane.

Example: Consider the dissociative EC process $CF_2Cl_2 + e^- \rightarrow F^- + CFCl_2^{\bullet}$. Let the potential energy of CF_2Cl_2 be zero. The homolytic bond dissociation energy $D_{(F–CFCl2)}$ has been calculated as 4.93 eV. Now, the potential energy of the products is 4.93 eV less the electron affinity of a fluorine atom ($EA_{(F\bullet)}$ = 3.45 eV), i.e., the process is endothermic by 1.48 eV. The experimental AE of the fragments is 1.8 eV. This yields a minimum excess energy of 0.32 eV (Fig. 7.13). [79]

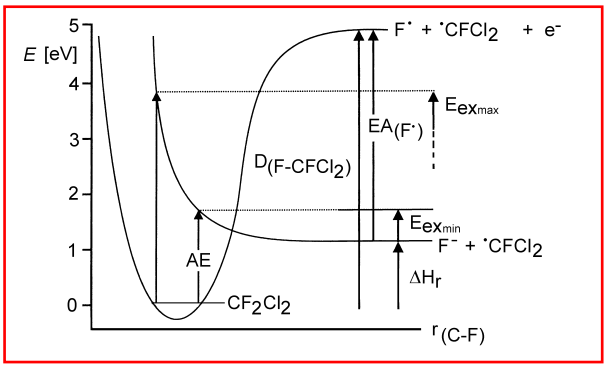

Fig. 7.13. Potential energy diagram of dissociative EC process $CF_2Cl_2 + e^- \rightarrow F^- + CFCl_2^{\bullet}$.

Table 7.3. Selected electron affinities [80]

Compound	EA [eV]	Compound	EA [eV]
carbon dioxide	–0.600	pentachlorobenzene	0.729
naphthalene	–0.200	carbon tetrachloride	0.805
acetone	0.002	biphenylene	0.890
1,2-dichlorobenzene	0.094	nitrobenzene	1.006
benzonitrile	0.256	octafluorocyclobutane	1.049
molecular oxygen	0.451	pentafluorobenzonitrile	1.084
carbon disulfide	0.512	2-nitronaphthalene	1.184
benzo[e]pyrene	0.534	1-bromo-4-nitrobenzene	1.292
tetrachloroethylene	0.640	antimony pentafluoride	1.300

7.4.4 Creating Thermal Electrons

Thermionic emission from a heated metal filament is the standard source of free electrons. However, those electrons usually are significantly above thermal energy and need to be decelerated for EC. Buffer gases such as methane, isobutane, or carbon dioxide serve well for that purpose, but others have also been used. [64,74,81] The gases yield almost no negative ions themselves while moderating the energetic electrons to thermal energy. [69] Despite inverse polarity of the extraction voltage, the same conditions as for PICI can usually be applied (Fig. 7.12). However, EC is comparatively sensitive to ion source conditions. [67,82] The actual ion source temperature, the buffer gas, the amount of sample

Example: The reduced sample consumption of nanoESI allows for the sequencing of the peptides (Chap. 9.4.7) obtained by tryptic digestion of only 800 fmol of the protein bovine serum albumin (BSA, Fig. 11.6). [66] The experiment depicted below requires each of the BSA-derived peptide ions in the full scan spectrum to be subjected to fragment ion analysis by means of CID-MS/MS on a triple quadrupole instrument (Chaps. 2.12 and 4.4.5).

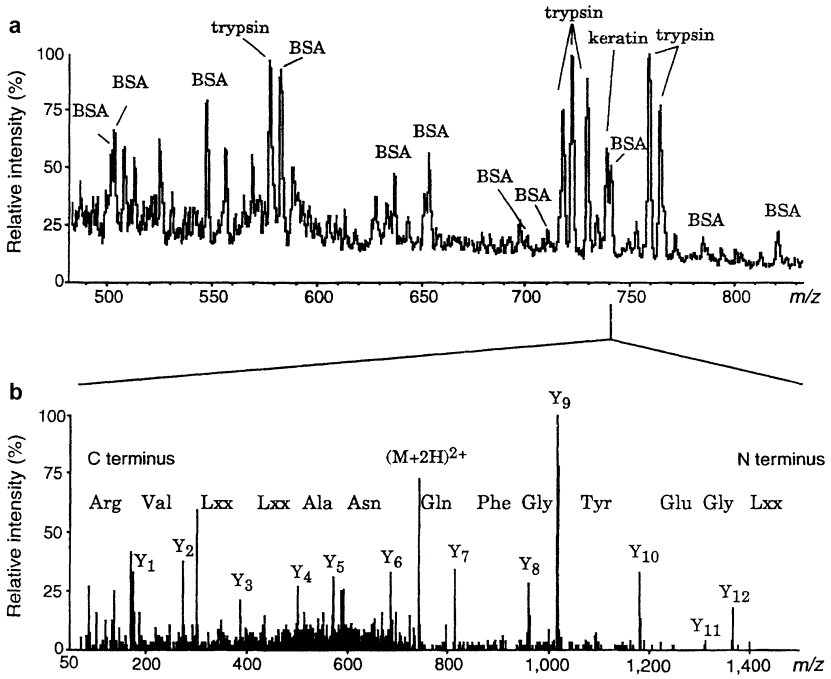

Fig. 11.6. Peptide sequencing by nanoESI-CID-MS/MS from a tryptic digest of bovine serum albumin (BSA); 800 fmol of BSA were used. (**a**) Full scan spectrum, (**b**) fragmentation of the selected doubly charged peptide ion at *m/z* 740.5. Adapted from Ref. [66] by permission. © Nature Publishing Group, 1996.

Note: Besides its low sample consumption, nanoESI is free of *memory effects* because each sample is supplied in a fresh capillary by means of disposable micropipettes. Furthermore, the narrow exits of nanoESI capillaries prevent air-sensitive samples from rapid decomposition.

11.2.3.1 Nano-Electrospray from a Chip

The sample throughput of nanoESI is limited by the comparatively time-consuming procedure of manual capillary loading. A chip-based nanoESI sprayer on an etched silicon wafer allows for the automated loading of the sprayer array by a pipetting robot (Fig. 11.7). The chip provides a 10×10 array of nanoESI